

Fig. 1 Nichols Chart plot (log magnitude-phase) of open loop tracking bounds $q(\omega)$ for the Example of Eq. (17) including the minimum phase nominal loop transmission function $L_{m0}(j\omega)$ (labeled $L(\omega)$ in the figure) based upon the initial feasible controller of Eq. (19)

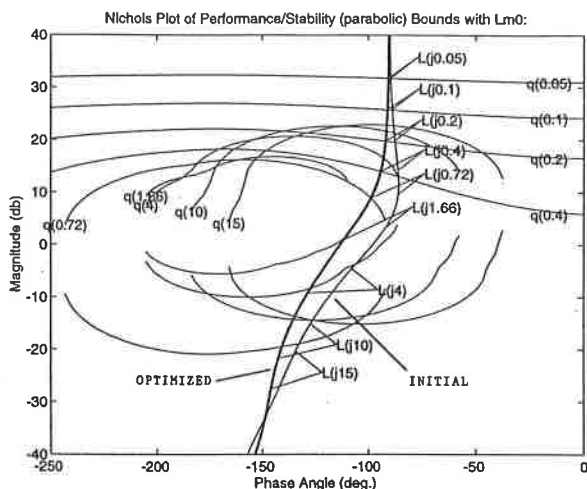


Fig. 2 Nichols Chart plot of Example of Eq. (17) illustrating the minimum phase nominal loop transmission functions $L_{m0}(j\omega)$ based upon the initial feasible controller of Eq. 19 (narrow line) and the optimized controller of Eq. 20 (heavy line)

iteration violates Nyquist stability, at which point the designer must choose to modify the controller structure or stop. Cost function weights a_0 , a_1 , and a_2 can also be varied, as suggested in Section 3, so that a set of Pareto-optimal solutions is obtained.

6 Conclusions

In this paper, the feasibility of extending the nonlinear programming method to the sensitivity-based, new formulation QFT problem of Nordgren et al. (1994) has been demonstrated. Although it was not possible to obtain analytic expressions for sensitivity-based QFT constraints or their gradients, it was shown that acceptable solutions could be obtained by use of spline approximations. The key step involved construction of a "hybrid" constraint gradient expression (part analytical, part numerical) which was found to yield superior convergence properties. This finding is also applicable to parameter optimization for fixed-structure controllers based upon bounds of a general nature, such as those developed in traditional, template-based QFT (i.e., without template approximation). Future work in this area will focus on the application of these techniques to MIMO systems (a straightforward extension) and discrete-time systems.

Acknowledgments

The author would like to express his appreciation to Dr. Richard E. Nordgren of Westvaco Corp., Covington, VA, and to the anonymous reviewers for their helpful suggestions. This work was supported in part by a grant from the University of Cincinnati Research Council.

References

- Bailey, F. N., Helton, J. W., and Merino, O., 1995, "Generation of Worst Case Performance Functions in Loop Gain-Phase Shaping," *Quantitative and Parametric Feedback Theory Symp. Proc.*, Purdue University, West Lafayette, IN.
- Chait, Y., Borghesani, C., and Zheng, Y., 1995, "Single-Loop QFT Design for Robust Performance in the Presence of Non-Parametric Uncertainties," *ASME JOURNAL OF DYNAMIC SYSTEMS, MEASUREMENT AND CONTROL*, Vol. 117, pp. 420-425.
- Horowitz, I. M., 1973, "Optimum Loop Transfer Function in Single-Loop, Minimum Phase Feedback Systems," *International J. of Control*, Vol. 22, pp. 97-113.
- Horowitz, I. M., and Sidi, M., 1972, "Synthesis of Feedback Systems with Large Plant Ignorance for Prescribed Time Domain Tolerance," *International J. of Control*, Vol. 16, pp. 287-309.
- Jayasuriya, S., and Zhao, Y., 1994, "Stability of Quantitative Feedback Designs and the Existence of Robust QFT Controllers," *International J. of Robust and Nonlinear Control*, Vol. 4, pp. 21-46.
- Nordgren, R. E., Nwokah, O. D. I., and Franchek, M. A., 1994, "New Formulations for Quantitative Feedback Theory," *International J. of Robust and Nonlinear Control*, Vol. 4, pp. 47-64.
- Thompson, D. F., and Nwokah, O. D. I., 1994, "Analytic Loop Shaping Methods in Quantitative Feedback Theory," *ASME JOURNAL OF DYNAMIC SYSTEMS, MEASUREMENT, AND CONTROL*, Vol. 116, pp. 169-177.
- Zhao, Y., and Jayasuriya, S., 1994, "On the Generation of QFT Bounds for General Interval Plants," *ASME JOURNAL OF DYNAMIC SYSTEMS, MEASUREMENT, AND CONTROL*, Vol. 116, pp. 618-627.

Comparison and Validation of Dynamics Simulation Models for a Structurally Flexible Manipulator

Jeff Stanway,¹ Inna Sharf,¹ and Chris Damaren²

This paper presents a series of experimental results obtained with a 2-DOF flexible-link direct-drive manipulator. First, we conduct a frequency analysis by comparing experimental natural frequencies with those predicted by the finite element model. Then, the time responses from four dynamics models are compared with each other and with the experiment. It is demonstrated that higher order nonlinearities are less important for slow maneuvers by close agreement between all four simulation models. For fast maneuvers, the two simpler models fail to predict a physically meaningful response. Good agreement with experimental results is attained with a model which accounts for all inertial nonlinearities. It is also shown that inclusion of damping in the dynamics models has a significant impact on their performance, as well as improving the correlation with experimental data.

¹ Graduate Student and Associate Professor respectively, Department of Mechanical Engineering, University of Victoria, Victoria, British Columbia, Canada V8W 3P6.

² Senior Lecturer, Department of Mechanical Engineering, University of Canterbury, Private Bay 4800, Christchurch, New Zealand.

Contributed by the Dynamic Systems and Control Division of THE AMERICAN SOCIETY OF MECHANICAL ENGINEERS. Manuscript received by the Dynamic Systems and Control Division June 12, 1996. Associate Technical Editor: T. Alberts.

1 Introduction

An accurate model for simulation of structurally flexible manipulators is a low cost alternative to prohibitively expensive space- or ground-based facilities. Validating a dynamics model for use in simulation or control is an important step before the model can be employed with confidence. Typically, model validation can be considered in two parts. The first—frequency domain analysis—is a natural place to begin. Matching of the natural frequencies is a good indication of accurately modeled mass and stiffness properties. The convergence rate of the numerical mode shapes to those observed usually reflects the accuracy of the chosen deformation model. However, as reported by many researchers, the frequency response and mode shapes can be significantly affected by damping and friction. The works by Hastings and Book (1986), Swevers et al. (1992) and Nebot et al. (1994) conduct frequency analysis for a single-link arm while Oakley and Cannon (1989) verify a set of assumed mode shapes for a two-link flexible arm.

The second part of model validation is the time domain analysis. Here, the focus is on time response of various system states to some control inputs. Time domain results show the effects of assumptions concerning the nonlinear terms in the motion equations as well as the geometric stiffening. As demonstrated in Chapnik et al. (1991) and Oakley and Cannon (1988), modeling of hub friction and link (structural) damping is also important in the time domain.

A number of time domain validations reported in the literature are conducted with a PD feedback controller in the simulation and experimental setup. For example, Lucibello and Ulivi (1993) use feedback during the validation of a dynamics model for a two-link rigid-flexible manipulator. Oakley and Cannon (1988) have also used feedback control when validating an assumed modes model for a two-link robot with a flexible forearm. Carusone et al. (1993) used square and circular end-point trajectories to test a tracking controller for a two-link flexible manipulator.

A validation study conducted under *open-loop* control provides a better scenario since the use of feedback tends to mask some of the effects present in the system. An accurate agreement for displacement variables is the most difficult to achieve but has been attained for impact dynamics of a flexible beam by Chapnik et al. (1991). Validation of acceleration and strain responses is easier to accomplish but it hides the rate errors. Giovagnoni (1994) compared both tip acceleration and strains for a flexible four-bar linkage and obtained excellent results. Similarly, Pal and Ohtsubo (1994) compared tip accelerations of a single-link flexible arm with rotary and prismatic actuation.

In this paper, we validate the dynamics models of a planar 2-DOF manipulator with two flexible links. The models considered here are described in Damaren and Sharf (1995) where a detailed classification of the nonlinearities in the dynamics equations and corresponding definitions of the four dynamics models is given. Summarizing, the first group of nonlinear terms identified are the inertial nonlinearities which include quadratic rate nonlinearities (δf) and the elastic dependence of each body's mass matrix (δM). The geometric elastic nonlinearities result from the use of geometrically nonlinear elastic theory, in particular, the nonlinear strain-displacement relations. They account for link foreshortening and the geometric stiffness effect due to high axial loading on the manipulator links. The last category of nonlinear terms contains the geometric interbody nonlinearities which are classified according to the approximation adopted for the interjoint position vector and interbody elastic rotation. Several approximations are possible which account for these deformations in three dimensions but they are equivalent for the planar motion ultimately considered here.

Based on this classification of nonlinear terms, Damaren and Sharf (1995) defined four dynamics models distinguished by the complexity of the nonlinear terms retained. These are the

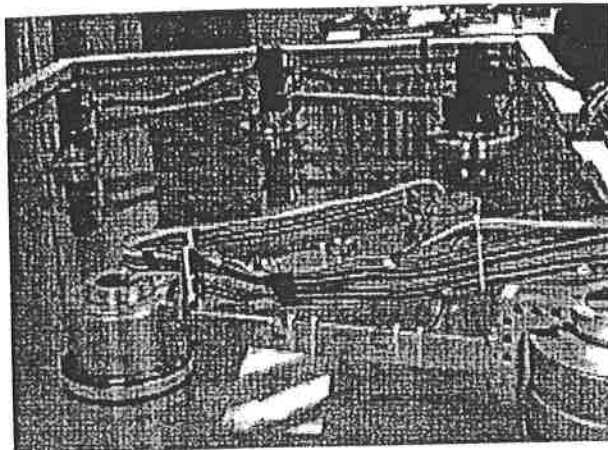


Fig. 1 Cooperating manipulator test-bed

Ruthlessly Linearized (RL), Inconsistent (I), Consistently Linearized (CL) and Exact (EE) models. The RL model contains only rigid-body nonlinearities while the I model retains all the inertial nonlinearities (the δf and δM terms). The CL approximation includes the nonlinear inertial forcing (δf) terms and the geometric stiffness matrix derived under a constant axial load assumption but neglects the δM terms. Finally, the EE model is the full embodiment of the nonlinear dynamics equations. In this paper, all four models are based on the finite element discretization of the flexible manipulator links.

The main contribution of this paper is to conduct frequency and time domain validations with an experimental flexible-link manipulator. Following a brief description of the test-bed, we examine the natural frequencies of the manipulator in an outstretched configuration. Subsequently, an open-loop time domain validation is conducted for smooth and step maneuvers executed at two different speeds. The simulation results from the aforementioned dynamics models are compared to the experimental joint rates and strain gauge measurements.

2 Experimental Facility

2.1 Overview. Since the experimental validation described in this paper was conducted with the Cooperating Manipulator test-bed at the University of Victoria, a brief overview of this facility is in order. A detailed description of the test-bed can be found in Nahon et al. (1995).

The test-bed was built to support research in dynamics and control of cooperating and structurally flexible manipulators in the null-gravity environment of space. As shown in Fig. 1, the facility is composed of two 3-DOF arms supported on a glass table. The elbow and wrist joints of the arms float on air bearings while the base of each arm is held down by a vacuum. The manipulator has a modular architecture which permits any combination of motors and links. The arm used for this work (foreground in Fig. 1) is driven by three direct-drive NSK Megatorque motors, models 1010, 0608, and 0408. In the present experiments, only the base and elbow motors of the arm are actuated. In addition to the flexible-link configuration shown in the figure, rigid links are also used for torque calculation as described in Section 4.2.

The control system consists of a PC-hosted Spectrum TMS320C30 floating-point digital signal processor interfaced to the robot through three 2-axis DS-2 Controller/Data Acquisition Modules from Integrated Motions Inc. In addition, three in-house interface boards were built to mediate between each DS-2 card and the motor driver units they service. The driver units for the NSK motors have position, velocity, and torque control options. Homing was accomplished in position mode

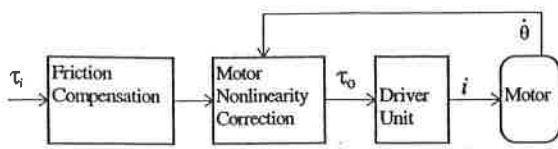


Fig. 2 Motor torque correction

while the experiments were conducted with direct torque commands.

Each of the flexible links is equipped with two sets of strain gauges (on both sides of the links) located at $\frac{1}{3}$ and $\frac{2}{3}$ length. Bridge Amplifier Modules from Analog Devices complete the bridge and provide electrical isolation and surge protection. Acquisition of the strain gauge data is provided by a 32 channel A/D converter. The joint angles of the motors are read from encoders built into the motors. For the joint rate input used in the motor nonlinearity correction in Fig. 2, a simple finite difference estimate of the joint velocity is used.

The simulation algorithm requires that the inertias and geometric properties of each body in the manipulator be modeled separately. The major components of the experimental arm are the links, couplers, motor housings, rotors and air bearings. The inertial properties of these were computed analytically for the simple bodies and by solid AutoCAD modeling for the complex bodies. In all, a 12-body model of the arm, detailed in Shepard (1994), was created for use in the simulation. The flexible aluminum links were modeled using planar beam elements with a stretch (axial) degree of freedom included. The latter is required in order to capture the geometric stiffening effect through the nonlinear stiffness formulation, as described in Sharf (1996). It is also required in a similar geometrically nonlinear formulation derived independently by Mayo and Dominguez (1996). As expected, the inclusion of high-frequency stretch degree of freedom significantly increases the computational cost of the simulation.

2.2 Motor Calibration. The time domain experiments with the manipulator were conducted under open-loop torque control. It was therefore necessary to calibrate the motors for accurate achievement of the torque commands. The calibration procedure involved accelerating each motor with a known load and calculating the shaft torque. Input-output torque relations were constructed for the motor/driver system. Nonlinear effects such as velocity dependence, motor/generator operation, directional dependence and command scale nonlinearities were taken into account (see Stanway (1996) for details). Due to the highly nonlinear characteristics of the NSK motors, the calibration was not sufficient to provide the desired accuracy of output torque. Nonetheless, the calibration is used to partly linearize the motors (Fig. 2) but another means of obtaining the output torque profiles is described in Section 4.2.

Motor friction was identified by observing each motor decelerate to a stop with a known inertial load under zero torque input. The tests showed a dominant Coulomb friction and a weak first-order effect, each with a small directional dependence. All three effects are included in the friction model of Fig. 2.

3 Frequency Domain Validation

The global form of the motion equations can be written as

$$\mathbf{M}(\mathbf{q})\ddot{\mathbf{q}} + \mathbf{D}\dot{\mathbf{q}} + \mathbf{K}(\mathbf{q})\mathbf{q} = \mathbf{B}\boldsymbol{\tau} + \mathbf{f}_{non}(\mathbf{q}, \dot{\mathbf{q}})$$

where \mathbf{M} , \mathbf{D} , and \mathbf{K} are the global mass, stiffness, and damping matrices respectively, the generalized coordinates are $\mathbf{q} = [\boldsymbol{\theta}^T \mathbf{q}_e^T]^T$, $\boldsymbol{\tau}$ are the joint torques, and \mathbf{f}_{non} is a vector of rate nonlinearities. Here, $\boldsymbol{\theta}$ are the joint angles and \mathbf{q}_e are the elastic coordinates generated with clamped-free boundary conditions

Table 2 Unconstrained natural frequencies [Hz]

Frequency source	Mode 1	Mode 2	Mode 3	Mode 4
FE Model, no damping	9.16	20.7	26.7	57.2
Impact experiment	8.30	17.6	24.9	50.7
FE Model, damping	8.83	17.6	26.7	50.5

for each link. The undamped, unconstrained (joints unlocked) natural frequencies were found by solving the global eigenproblem for the linearized arm model:

$$-\omega_\alpha^2 \mathbf{M}(\bar{\mathbf{q}})\mathbf{q}_\alpha + \mathbf{K}(\bar{\mathbf{q}})\mathbf{q}_\alpha = \mathbf{0}, \quad \alpha = 1, 2, 3, \dots \quad (1)$$

where ω_α are the natural frequencies, \mathbf{q}_α are the mode shapes, and $\bar{\mathbf{q}}$ is the reference configuration. The experimental natural frequencies were determined by an impact to the elbow motor. The strain and joint angle data were collected at a sampling rate of 1000 Hz. The elbow joint rate was obtained by differentiating the angle measurements. The experimental frequencies reported in Table 2 correspond to the peaks of the elbow rate curve in Fig. 3. As can be seen from Table 2, the two sets agree within 10–15 percent in the absence of damping. We also observed that both numerical and experimental frequencies changed little with the arm configuration (Damaren et al., 1995). This is one of the consequences of the direct-drive actuation of the experimental arm.

So as to include damping in the model, the system damping factors were obtained by exciting the manipulator at the natural frequencies from the elbow motor and measuring the vibration decay. The damping ratios ζ_α for each mode were calculated from the joint angles and strain measurements by using logarithmic decrement. The data were passed through a high pass filter to remove the influence of drift and the low frequency cantilever modes of the arm caused by joint friction.

The estimated damping ratios for the first four vibration modes were found to be $\zeta_1 = 0.13$, $\zeta_2 = 0.06$, $\zeta_3 = 0.07$, and $\zeta_4 = 0.06$. These were used to define modal damping and subsequently, the damping matrices for the two flexible links. Thus, all damping effects have been effectively incorporated via the structural damping in the links. Letting \mathbf{Q} represent the matrix of eigenvectors corresponding to the eigenproblem (1), we note that it diagonalizes \mathbf{M} and \mathbf{K} according to $\mathbf{Q}^T \mathbf{M} \mathbf{Q} = \text{diag}\{1\}$ and $\mathbf{Q}^T \mathbf{K} \mathbf{Q} = \text{diag}\{\omega_\alpha^2\}$. \mathbf{Q} and the global damping matrix can be further partitioned as

$$\mathbf{Q} = \begin{bmatrix} \mathbf{Q}_{\theta\theta} & \mathbf{Q}_{\theta e} \\ \mathbf{0} & \mathbf{Q}_{ee} \end{bmatrix}, \quad \mathbf{D} = \begin{bmatrix} \mathbf{0} & \mathbf{0} \\ \mathbf{0} & \mathbf{D}_{ee} \end{bmatrix} \quad (2)$$

where $\mathbf{Q}_{\theta\theta}$ are the joint angles in the zero-frequency rigid modes, \mathbf{Q}_{ee} are elastic coordinates in the elastic modes, and $\mathbf{Q}_{\theta e}$ are the

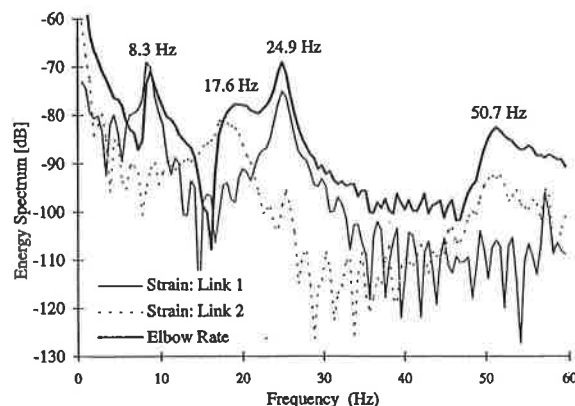


Fig. 3 Frequency response to elbow motor impact

joint angles in those modes. Assuming that Q also diagonalizes D , we can write $Q_{ee}^T D_{ee} Q_{ee} = \text{diag} \{2\zeta_\alpha \omega_\alpha\}$ or

$$D_{ee} = Q_{ee}^{-T} \text{diag} \{2\zeta_\alpha \omega_\alpha\} Q_{ee}^{-1} \quad (3)$$

Thus, the damping matrix for the manipulator is calculated as in the above with the four measured values of the damping ratios ζ_α . The body damping matrices for the body motion equations are defined by truncating D_{ee} to a block-diagonal form.

The modal damping factors ζ_α were measured at the outstretched configuration of the arm and hence, Q_{ee} was evaluated at this configuration. We note that Q_{ee} does not vary much with configuration so that D_{ee} is taken as constant. The damped numerical frequencies in Table 2, found by random torque excitation of the simulation, agree very well with the observed behavior.

4 Time Domain Analysis

In this section we compare the performance of the four models—Ruthlessly Linearized, Inconsistent, Consistently Linearized and Exact—against each other and the measured response.

4.1 Test Maneuvers. Two joint space test trajectories are considered, each executed at a high and a low speed. The first is a generic “pick-and-place” maneuver represented by a smooth fifth order polynomial and denoted by PP. The commanded joint angle in this case is given by

$$\theta_d(t) = (\theta_f - \theta_0) \frac{t^3}{T^3} [10 - 15(t/T) + 6(t^2/T^2)] \quad (4)$$

where $\theta_0 = \theta_d(0)$ is the initial angle and $\theta_f = \theta_d(T)$ is the desired final one. The second maneuver is a step acceleration (ST) designed to excite significant vibrations in the robot:

$$\ddot{\theta}_d(t) = \begin{cases} A, & 0 < t \leq T/2 \\ -A, & T/2 < t \leq T \\ 0, & t > T \end{cases}, \quad A = 4(\theta_f - \theta_0)/T^2 \quad (5)$$

This maneuver is also used to investigate the geometric stiffening effect.

In both of these maneuvers, the arm moves from the outstretched home position to the position with base and elbow joint angles at 2 and 1.5 radians, respectively. The high speed maneuvers, (-f), are completed in $T = 2.5$ seconds and bring the flexible links close to their elastic limits, while the 5 second slow maneuvers, (-s), are more gentle. We note that the terms “fast” and “slow,” used here to describe the maneuvers, are intended to have a relative meaning concurring with what one would perceive as a fast or a slow movement of the arm. The speed differences between the fast (PP-f, ST-f) and slow (PP-s, ST-s) maneuvers serve to accent the relative importance of various nonlinear terms in the dynamics equations. With the exception of the ST-f maneuver, the desired trajectories are converted into commanded joint torques via the rigid-body inverse dynamics model, as discussed below.

4.2 Shaft Torque Calculation. An alternative solution to motor calibration is proposed here to obtain an accurate estimate of the torque output from the motors. First, the desired maneuver is conducted under open-loop torque control (with motor correction as shown in Fig. 2) with a rigid-link configuration of the arm. The measured joint angles are low-pass filtered and differentiated off-line to obtain the joint velocities and accelerations. These are then used in the rigid-body dynamics model of the manipulator to calculate the actual torque output of the motors.

The torques calculated with the above procedure are subject to some error from loss of frequency content and small inaccuracies likely present in the manipulator model. Accordingly, they

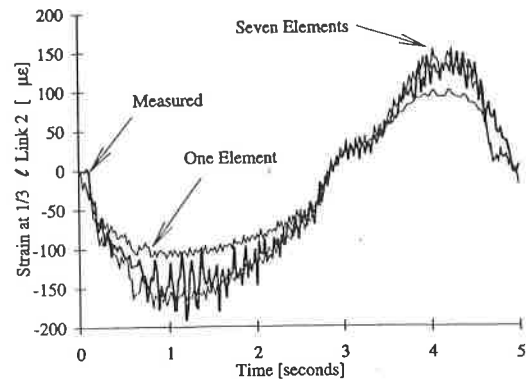


Fig. 4 Strain for link 2, PP-s maneuver, EE model

will be more accurate for the smooth polynomial maneuvers than the fast step acceleration maneuvers. In fact, they are considered to be the best estimates of the motor torques for the same maneuvers conducted with a flexible-link configuration of the arm. The calculated torques are used as control inputs to the simulation of smooth and slow step maneuvers.

4.3 Simulation Versus Experiment

Model Convergence. The convergence of the four models with increasing number of finite elements was investigated for the smooth and step acceleration maneuvers. It was observed that models RL, CL, and I converged within one element for the slow maneuvers and two or three elements for the fast maneuvers. The EE Model, on the other hand, exhibited a very slow convergence rate with the number of elements. This has been attributed to the nonlinear stiffness formulation employed to capture the geometric stiffening effect (Damaren and Sharf, 1995). As shown by Sharf (1994), the slow convergence of the exact dynamics model can be alleviated by using higher order shape functions for the stretch degree of freedom. Mayo and Dominguez (1996), using the same approach to model the geometric stiffness as in our exact model, reached similar conclusions regarding its convergence. They also point out the need for a very fine discretization with, preferably, higher-order axial shape functions. Figure 4 displays the measured and simulated strains for the second flexible link for the slow polynomial maneuver using the EE model. We note that the converged (7-element) solution is in good agreement with the experimental results, but it requires approximately two days of CPU time to compute on a Sun 4 workstation.

Slow Maneuvers. Figures 5 and 6 compare the numerical results with strain and joint rate measurements for the slow smooth (PP-s) maneuver. In these figures, we show the converged results for the RL and I models and the seven-element solutions for the EE model. The CL model is omitted for clarity and because its solutions are nearly identical to the I model results. Also, the simulated responses shown in these figures were calculated without damping in order to expose the effect of various nonlinearities in the motion equations.

As can be seen from Fig. 5, the RL and I models predict similar responses which are in good agreement with the measured strains. The EE model slightly underestimates the strains. From Fig. 6, one can conclude that the EE model provides the best frequency match with experiment while the RL and I models overestimate the vibration amplitude. Figure 7 is the analogue of Fig. 5, but obtained with damping in the models. As expected, damping diminishes the differences between the various models. Overall, the solutions calculated with damped models are in better agreement with experiment. It follows that the high order nonlinear dynamics terms are not important for slow maneuvers, although in the absence of the damping term, they

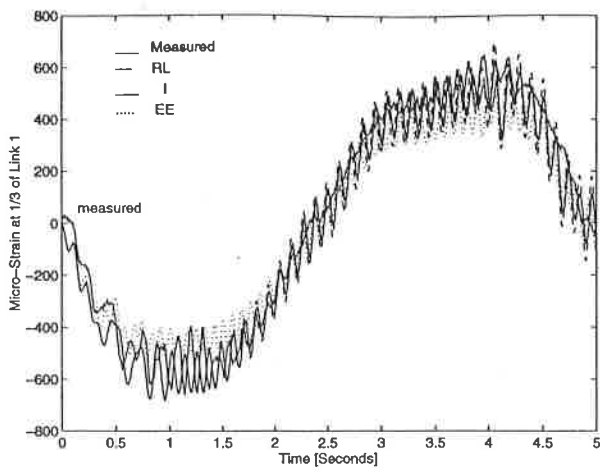


Fig. 5 Strain for link 1, PP-s maneuver, undamped models

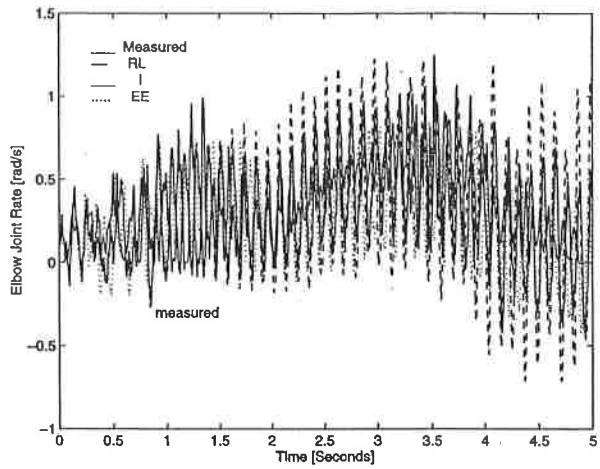


Fig. 6 Elbow joint rate, PP-s maneuver, undamped models

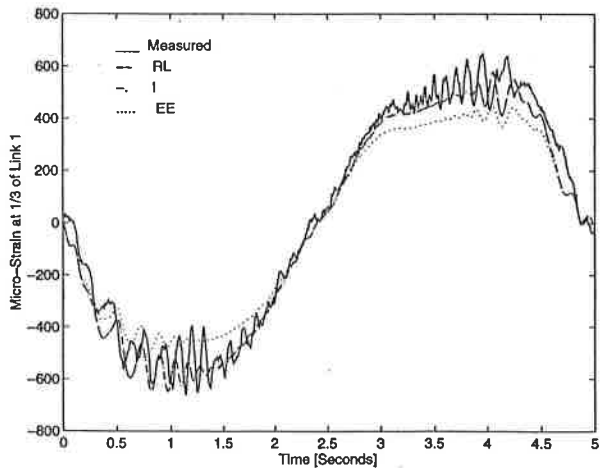


Fig. 7 Strain for link 1, PP-s maneuver, damping

produce visible differences in the response. The strain results for the slow step maneuver (ST-s) in Fig. 8 were obtained with damping included in the models and lead to similar conclusions on their performance.

Fast Maneuvers. Strain and elbow joint rate results for the fast smooth (PP-f) maneuver are shown in Figs. 9 and 10, respectively, where (a) present the undamped solutions, while

(b) contain the damped simulated responses. With or without damping, the CL model does not complete this maneuver. For the RL model, in the undamped case, it accumulates a very high energy drift (22 percent) and hence, is not included in Figures 9(a) and 10(a). In the damped case, it performs better (7 percent energy drift at the end), although, as can be seen

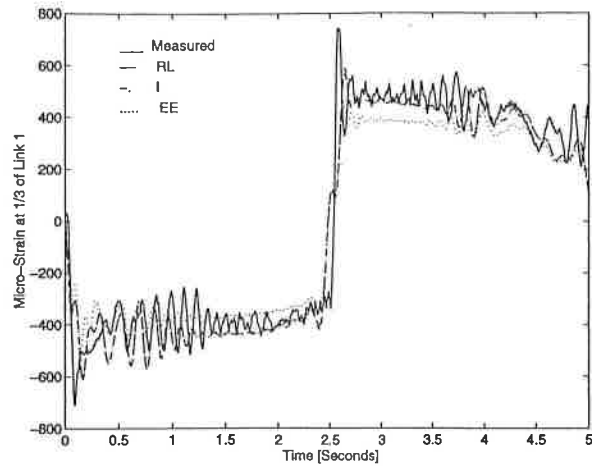


Fig. 8 Strain for link 1, ST-s maneuver, damping

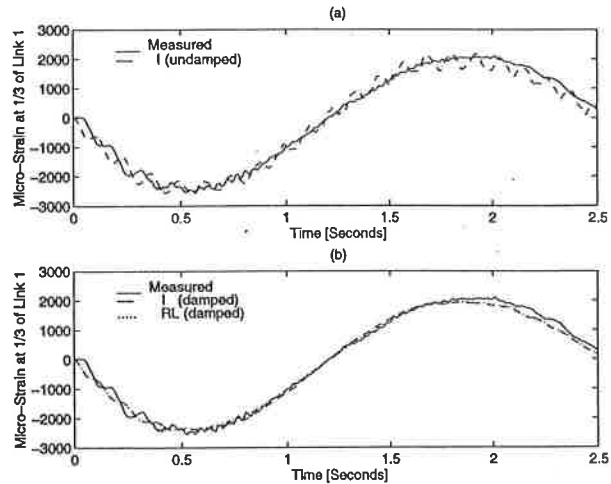


Fig. 9 Strain for link 1, PP-f maneuver

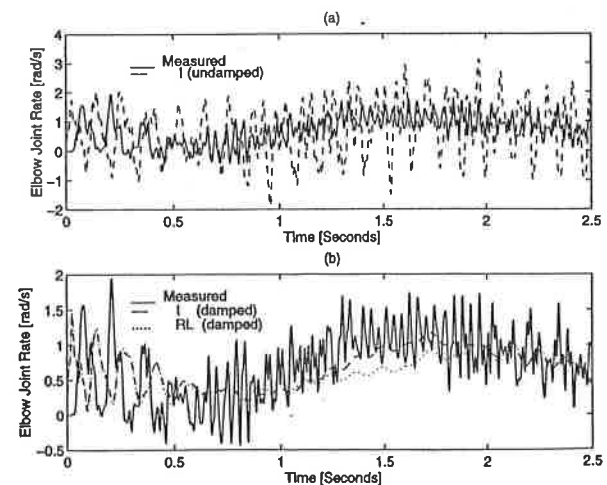


Fig. 10 Elbow joint rate, PP-f maneuver

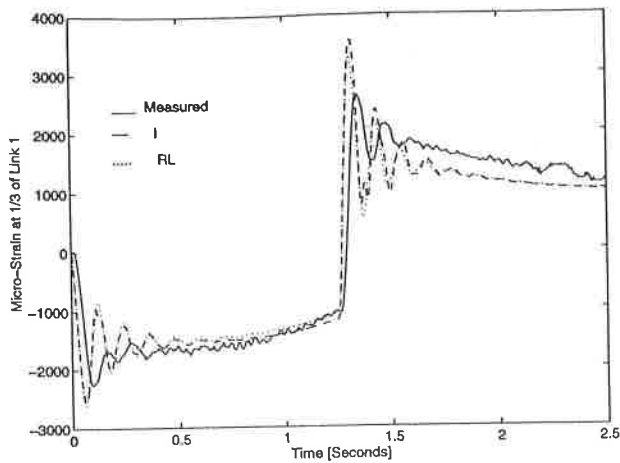


Fig. 11 Strain for link 1, ST-f maneuver, damping

from the joint rate in Fig. 10(b), its predictions are not reliable. Because of the slow convergence, we were unable to obtain converged solutions for the EE model and hence, it is not included in these graphs. As observed from Figs. 9 and 10, the responses calculated with the I model are consistently in good agreement with the experiment, although in the damped case, the joint rates are slightly overdamped.

As alluded earlier, the calculated torque inputs do not properly capture the sharp changes in the torque command for step acceleration maneuvers. Therefore, for a better comparison of fast step maneuvers, simulation results for the ST-f maneuver are obtained with the commanded torque rather than the calculated torque. Also, the damping term is included in the dynamics equations without which models RL and I cannot complete the maneuver. The CL model once again fails to produce a meaningful solution in either case. In the strain response of the first link in Figure 11, we observe an error in the absolute response (due to the error in the output torque of the motors), but well preserved torque steps. The RL and I models are again in close agreement, with the ruthlessly linearized model predicting larger amplitudes for the joint rates (Fig. 12). Both models predict a higher vibration frequency at the start and mid-way steps than what is measured. Barring these two discrepancies, the agreement with the experimental results is good. We therefore conclude that the geometric stiffening effect (not included in the RL and I models) is not important for the direct-drive experimental arm for a wide range of maneuvers.

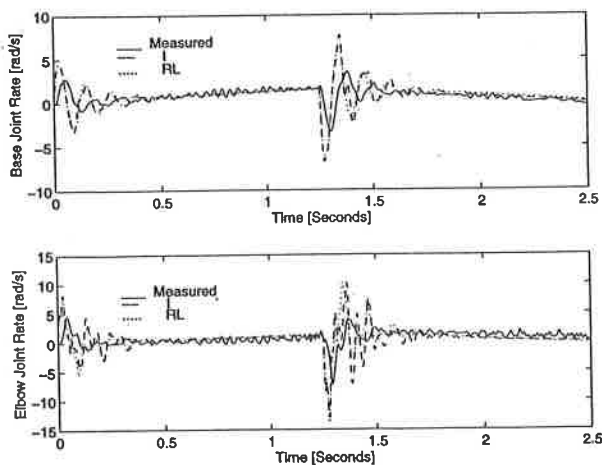


Fig. 12 Joint rates, ST-f maneuver, damping

5 Conclusions

In this paper, we have discussed the validation of the dynamics modeling for a 2-DOF manipulator with two flexible links. This included a comparison of numerically calculated frequency response with experiment as well as the time domain analysis. In the latter case, we compared the performance of four dynamics models ranging from the ruthless (RL) model which retains only rigid-body nonlinearities to the exact (EE) model which accounts for the geometric stiffening effect. It was found that the latter model exhibits a poor convergence rate—a limitation which prevents us from making definitive conclusions on its predictions. The relative importance of the nonlinear inertial terms was demonstrated by the virtually identical response of the models for the slow maneuver, and very different responses for the fast maneuver. Finally, structural damping is shown to be a necessary addition to the models for accurate prediction of the manipulator behaviour. The importance of the nonlinear inertial terms decreases considerably in the presence of damping. Overall, we conclude that the inconsistent (I) model is most reliable and provides the best agreement over a large range of maneuvers for the class of systems studied here. However, relative to the simpler ruthless model, its implementation requires a number of additional integrals of the shape functions (contributing to the δf and δM terms) and it takes approximately 10 to 20 percent extra CPU time to compute.

References

- Carusone, J., Buchan, K. S., D'Eleuterio, G. M. T., 1993, "Experiments in End-Effector Tracking Control for Structurally Flexible Space Manipulators," *IEEE Trans. on Robotics and Automation*, Vol. 9, No. 5, pp. 553-560.
- Chapnik, B. V., Heppler, G. R., and Aplevich, J. D., 1991, "Modeling Impact on a One-Link Flexible Robotic Arm," *IEEE Trans. on Robotics and Automation*, Vol. 7, No. 4, pp. 479-488.
- Damaren, C., and Sharf, I., 1995, "Simulation of Flexible-Link Manipulators With Inertial and Geometric Nonlinearities," *ASME JOURNAL OF DYNAMIC SYSTEMS, MEASUREMENT, AND CONTROL*, Vol. 117, pp. 74-87.
- Damaren, C. J., Stanway, J., and Sharf, I., 1995, "Modal Analysis for an Experimental Flexible Manipulator," *Proc. 15th Canadian Congress on Applied Mechanics, CANCAM'95*, Vol. 2, pp. 806-807.
- Giovagnoni, M., 1994, "A Numerical Example and Experimental Analysis of a Chain of Flexible Bodies," *ASME JOURNAL OF DYNAMIC SYSTEMS, MEASUREMENT, AND CONTROL*, Vol. 116, pp. 73-80.
- Hastings, G. G., and Book, W. J., 1986, "Verification of a Linear Dynamic Model for Flexible Robotic Manipulators," *Proc. of IEEE Int. Conf. on Robotics and Automation*, Vol. 2, pp. 1024-1029.
- Lucibello, P., and Ulivi, G., 1993, "Design and Realization of a Two-Link Direct-Drive Robot With a Very Flexible Forearm," *Int. J. Robotics and Automation*, Vol. 8, No. 3, pp. 113-128.
- Mayo, J., and Dominguez, J., 1996, "Geometrically Non-Linear Formulation of Flexible Multibody Systems in Terms of Beam Elements: Geometric Stiffness," *Computers and Structures*, Vol. 59, No. 6, pp. 1039-1050.
- Nahon, M., Damaren, C., Bergen, A., and Gonçalves, J., 1995, "A Test Facility for Multi-Armed Space-Based Manipulators," *Canadian Aeronautics and Space Journal*, Vol. 41, No. 4, pp. 391-400.
- Nebot, E. M., Lee, G. K. F., and Karim, N. M., 1994, "Parameter Identification for a Single-Link Flexible Manipulator," *Int. J. Modeling and Simulation*, Vol. 14, No. 3, pp. 139-144.
- Oakley, C. M., and Cannon, R. H. Jr., 1989, "Theory and Experiments in Selecting Mode Shapes for Two-Link Flexible Manipulators," *The First Int. Symposium of Experimental Robotics*, pp. 1-19.
- Oakley, C. M., and Cannon, R. H. Jr., 1988, "Initial Experiments on the Control of a Two-Link Manipulator With a Very Flexible Forearm," *Proc. of the American Control Conference*, pp. 996-1002.
- Chinmoy, P., and Hideomi, O., 1994, "Reduction of Tip Vibration of a 2-D Flexible Manipulator," *Journal of Intelligent Material Systems and Structures*, Vol. 5, pp. 30-41.
- Sharf, I., 1994, "A Higher-Order Geometrically Nonlinear Beam Element for Dynamics Simulation of Multibody Systems," *Proc. 12th Symposium on Engineering Applications of Mechanics*, pp. 569-578, McGill University, Montreal, Canada.
- Sharf, I., 1996, "Geometrically Nonlinear Beam Element for Dynamics Simulation of Multibody Systems," *Int. J. for Numerical Methods in Engineering*, Vol. 39, pp. 763-786.
- Shepard, D., 1994, "The Development of a Model for a Robotic Manipulator," Work Term Report, Department of Mechanical Engineering, University of Victoria.
- Stanway, J., 1996, "Validation of a Dynamics Simulation for a Structurally Flexible Manipulator," M.A.Sc. thesis, Department of Mechanical Engineering, University of Victoria, Victoria, Canada.
- Swevers, J., Torfs, D., Demeester, F., and Van Brussel, H., 1992, "Fast and Accurate Tracking Control of a Flexible One-Link Robot Based on Real-Time Link Deformation Measurements," *Mechatronics*, Vol. 2, No. 1, pp. 29-41.